Dalton Transactions

Electropolymerizable N-heterocyclic carbene complexes of Rh and Ir with enantiotropic polymorphic phases

Journal:	*Dalton Transactions*
Manuscript ID	DT-ART-12-2019-004844.R1
Article Type:	Paper
Date Submitted by the Author:	28-Jan-2020
Complete List of Authors:	Jones, Richard; University of Texas at Austin, Department of Chemistry Wang, Weiran; University of Texas at Austin, Department of Chemistry Lynch, Vincent; University of Texas at Austin, Chemistry Guo, Hongyu; University of Texas at Austin, Department of Chemistry Datta, Anwesha; University of Texas at Austin, Department of Chemistry

ARTICLE

Electropolymerizable N-heterocyclic carbene complexes of Rh and Ir with enantiotropic polymorphic phases.

Received 00th January 20xx,
Accepted 00th January 20xx

DOI: 10.1039/x0xx00000x

Weiran Wang, Vincent M Lynch, Hongyu Guo, Anwesha Datta and Richard A Jones*

New Rh (**1**) and Ir (**2**) complexes of an N-heterocyclic carbene (NHC) featuring a terthiophene backbone were synthesized. Single crystal X-ray diffraction studies of **1** and **2** at 100 K and 298 K respectively, revealed two enantiotropic polymorphic phases with similar lattice parameters for each compound. The transition temperature between two crystalline forms for each compound was determined by measuring the percentage of reflections with a different space group ranging from 100 K to 298 K. Both **1** and **2** were also found to catalyze the hydrogen transfer reaction. The conducting metallopolymers **poly-1** and **poly-2** were synthesized from oxidative electropolymerization of **1** and **2**, respectively, in CH_2Cl_2 electrolyte solution on indium tin oxide-(ITO) coated glass. The electrochromic properties of synthesized conducting metallopolymers were studied by UV-vis-NIR spectroelectrochemistry.

Introduction

Since the first stable crystalline N-heterocyclic carbene (NHC) was isolated by Arduengo *et al.*[1] in 1991, the number of transition metal complexes using an NHC as a ligand has skyrocketed, covering most of the metallic elements in the periodic table. NHCs are good σ-donor ligands with great structural versatility. Designing and synthesizing new functional NHC ligands should lead to metal complexes with new properties. Metal complexes can be synthesized by direct metalation with free NHC, transmetalation with corresponding NHC-Ag complexes and *in-situ* generation of free carbene when treated with base from the air-stable imidazolium salt. Previously, NHC-metal complexes modified with electropolymerizable thiophene derivatives have been used to prepare conducting metallopolymers (CMPs) which exhibit electrochromic behavior due to the generation of charge carrier species when electrochemically oxidized.[2]

Compounds having more than one crystalline form (polymorphs) are well known.[3] Organic polymorphs play a critical role in in the pharmaceutical industry, influencing drug manufacturability, efficiency and quality.[3-4] In comparison, fewer studies have focused on organometallic polymorphic compounds.[5] From the supramolecular perspective, polymorphic phases can arise from the rearrangement of intermolecular interactions resulting in different thermodynamically stable molecular packing patterns at different temperatures. These can be classified as packing polymorphs which have a transition at a specific temperature (range) between each enantiotropic form.[5] We have previously reported the terthiophene-backboned *N,N'*-dimethylimidazolium (**L, Scheme 1**) as the precursor for the corresponding NHC-Pd and Pt complexes which can be further electropolymerized onto indium tin oxide-(ITO) coated glass as polymer thin films. In the synthesized CMPs, the NHC-metal moiety is directly tethered to the polythiophene backbone through N atoms. These CMPs displayed reversible color changes when electrochemically oxidized which can be observed by naked-eye observations as well as UV-vis-NIR spectroelectrochemistry. Herein, we report the synthesis of a new NHC-Rh(cod)I (**1**) complex and NHC-Ir(cod)I (**2**) complex (cod = 1,5-cyclooctadiene) using *in-situ* deprotonation of **L** (Scheme 1). Single crystal X-ray diffraction studies of their molecular structures revealed that both complexes have two different crystalline phases at 100 K and 298 K, respectively. The two solid-state structures were determined to be different enantiotropic packing polymorph phases. An approximation of the transition temperature between the two enantiotropic systems of each complex was made by counting the number of crystallographic reflections that violated the C-centered crystal lattice using quick single crystal X-ray diffraction scans. We have also shown that **1** and **2** are catalytically active toward

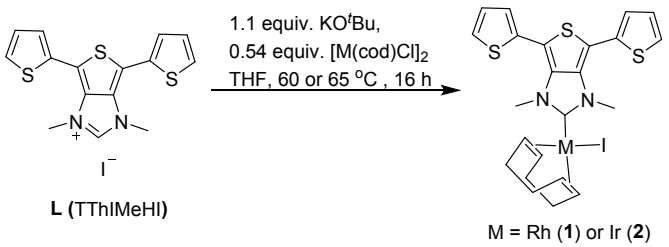

L (TThIMeHI)

Scheme 1. Synthesis of Rh (**1**) and Ir (**2**) NHC complex from **L**.

Department of Chemistry, The University of Texas at Austin, 105 E. 24th Street, Stop A5300, Austin, Texas 78712-1224, USA.

† Electronic Supplementary Information (ESI) available: CV of **poly-1** and **poly-2** in monomer free electrolyte solution, deconvoluted XPS spectra of **poly-1** and **poly-2**, text tables of crystallographic data and spectroscopic images for all new compounds (^{1}H NMR and ^{13}C NMR). See DOI: 10.1039/x0xx00000x

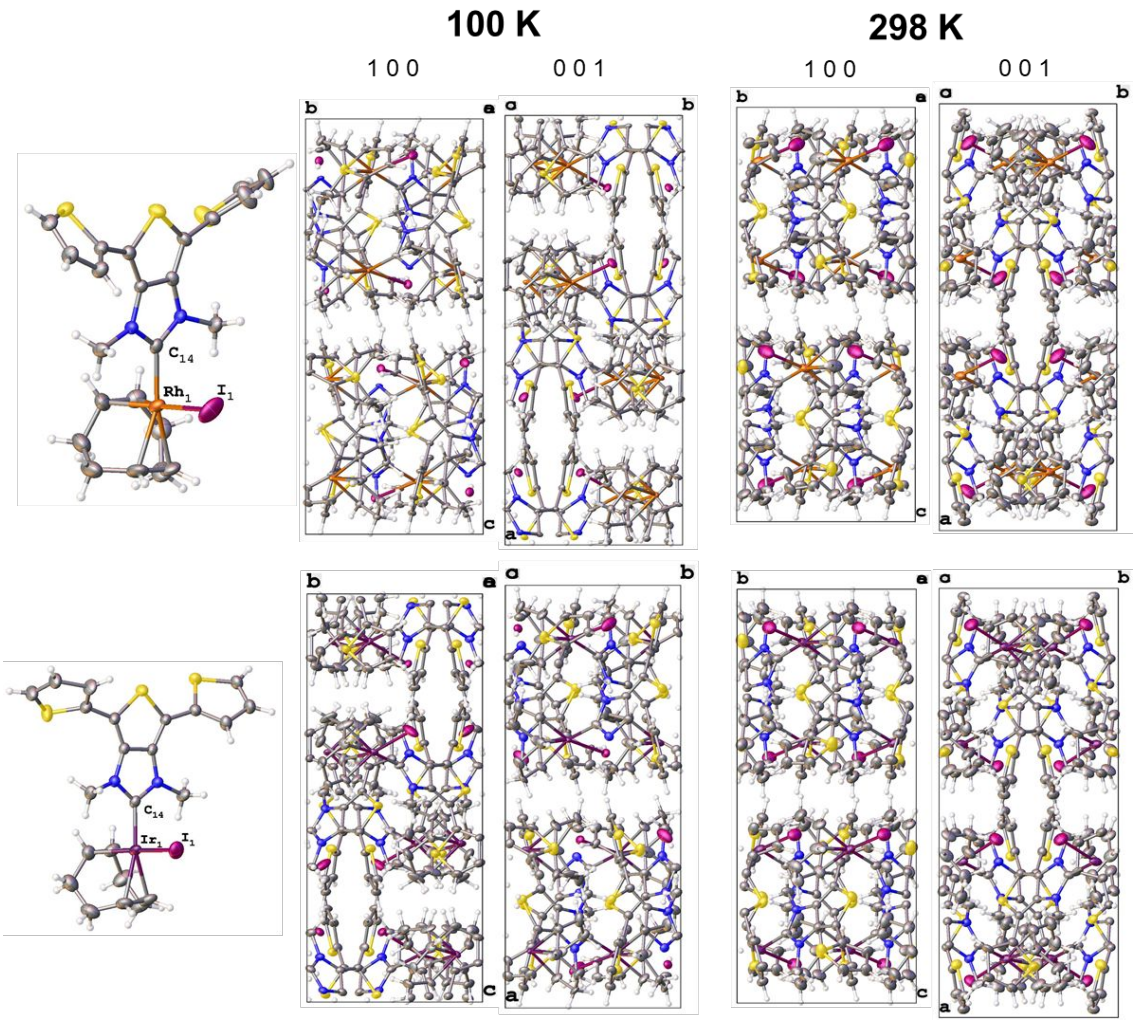

Fig. 1. Representative ORTEP views of **1** and **2** at 298 K showing the selective atom labelling scheme and their cell packing projections at 100 K and 298 K, as aligned along a-axis (1 0 0) and c-axis (0 0 1) direction. Displacement ellipsoids are scaled to the 30% level for structures at 298 K, and the 50% probability level for structures at 100 K. The minor components of the disordered thiophenes, iodide and cod moieties were omitted for clarity.

hydrogen transfer reactions. Like previously reported thiophene derivatives of functionalized salen[6] and NHC complexes[2], **1** and **2** can be converted to conducting metallopolymer thin films (**poly-1** and **poly-2**, respectively) by electrochemical oxidation using cyclic voltammetry (CV). The electrochromic properties of **poly-1** and **poly-2** were studied using UV-vis-NIR spectroelectrochemistry, which revealed a color change driven by the generation of charge carrier species (polaron and bipolaron).

Results and Discussions

Synthesis and single crystal X-ray diffraction studies

The imidazolium precursor (**L**, TThIMeHI) was prepared by a method established by our group.[7] The Rh and Ir NHC complexes, **1** and **2**, were prepared by the *in-situ* deprotonation/metalation of **L** using KO^{t}Bu as the base and Ir/Rh(cod)Cl dimer as the metal precursor in good yields (Scheme 1). ^{13}C-NMR studies confirmed the formation of Rh/Ir NHC complexes by their characteristic $C_{carbene}$ signal (δ = 213 ppm and 207 ppm, for Rh (**1**) and Ir (**2**) respectively). The solid-state crystal structure determinations of **1** and **2** were conducted at 298 K and 100 K. Table 1 shows crystal data and structure refinements at these two temperatures.

Fig. 1 shows the representative molecular structures of **1** and **2** at 298 K and the corresponding unit cell packing projection images as viewed along the a-axis (1 0 0) and c-axis (0 0 1) at each temperature. At 298 K, **1** and **2** are isostructural and crystallize in the monoclinic *C2/c* space group with one molecule in the asymmetric unit. They have similar unit cell parameters. Both the Rh and Ir metal centers possess distorted square planar geometries.

After data collection at 298 K the same crystals of **1** and **2** were also used for single crystal x-ray diffraction studies at 100 K which revealed the presence of new polymorphic forms. At the low temperature, **1** and **2** have the space groups $P2_1/a$ and

$P2_1/c$, respectively with two different molecules in the asymmetric unit. At 100 K, both **1** and **2** maintained the same molecular structure and had unit cell parameters which were similar to high temperature forms. Each structure had slightly decreased unit cell lengths, a wider β angle and a smaller unit cell volume as a result of the decrease in temperature from 298 K to 100 K.

The high temperature forms of both **1** and **2** have similar molecular packing at 298 K. At 100K, differences in packing patterns for each crystal can be observed. The same crystals of **1** and **2** were cycled between 100 K and 298 K several times, and the two polymorphic phases of each crystal were consistently observed. This confirmed that the two phases for each compound were enantiotropic polymorphic phases.

Table 1. Summary of Crystal data and structure refinement for **1** and **2** at 100 K and 298 K.

Compound	**1**	**1**	**2**	**2**
CCDC Number	1963645	1963646	1963647	1963648
T/K	100.02(10)	298.15	100.01(11)	298.15
Formula	$C_{23}H_{24}IN_2RhS_3$	$C_{23}H_{24}IN_2RhS_3$	$C_{23}H_{24}IIrN_2S_3$	$C_{23}H_{24}IIrN_2S_3$
FW/g.mol^{-1}	654.43	654.43	743.72	743.72
Crystal system	monoclinic	monoclinic	monoclinic	monoclinic
Space group	*$P2_1/c$*	*C2/c*	*$P2_1/a$**	*C2/c*
a/Å	24.032(2)	24.410(2)	24.1194(3)	24.425(2)
b/Å	9.1413(9)	9.2860(10)	9.17930(10)	9.2985(8)
c/Å	23.214(2)	23.474(2)	23.3012(4)	23.526(2)
α/°	90	90	90	90
β/°	113.241(4)	113.725(5)	113.303(2)	113.778(4)
γ/°	90	90	90	90
Volume/Å^3	4685.9(8)	4871.2(9)	4738.03(13)	4889.6(8)
Z	8	8	8	8
ρ_{calc} g/cm^3	1.855	1.793	2.085	2.021
μ/mm^{-1}	2.328	2.24	23.713	6.994
F(000)	2576	2600	2832	2832
Crystal size/mm^3	0.224 × 0.151 × 0.094	0.224 × 0.151 × 0.094	0.13 × 0.057 × 0.054	0.13 × 0.057 × 0.054
2Θ/°	1.844 to 57.182	4.066 to 56.808	7.394 to 175.606	3.644 to 57.02
Index ranges	-31 ≤ h ≤ 31 -12 ≤ k ≤ 12 -31 ≤ l ≤ 32	-31 ≤ h ≤ 32 -12 ≤ k ≤ 11 -18 ≤ l ≤ 31	-28 ≤ h ≤ 25 -11 ≤ k ≤ 11 -30 ≤ l ≤ 30	-32 ≤ h ≤ 32 -12 ≤ k ≤ 12 -31 ≤ l ≤ 31
Reflections collected	124829	20347	50416	52030
Independent reflections	11863 R_{int} = 0.0587 R_{sigma} = 0.0354	6023 R_{int} = 0.0539 R_{sigma} = 0.0797	9777 R_{int} = 0.0496 R_{sigma} = 0.0323	6150 R_{int} = 0.0619 R_{sigma} = 0.0473
Data/restraints /parameters	11863/586/565	6023/394/343	9777/618/653	6150/721/388
GOF on F^2	1.054	1.026	1.043	1.03
R_1, wR_2 [I≥2σ (I)]	0.0366, 0.0872	0.0542, 0.1185	0.0455, 0.1130	0.0316, 0.0670
R_1, wR_2 (all data)	0.0521, 0.0951	0.1151, 0.1394	0.0554, 0.1250	0.0571, 0.0738

*The crystal structure was first collected and solved as *$P2_1/c$*, but in order to compare with other structures, the a and c axial was switched by using WingGX[8] and the space group of **1** is finally reported as *$P2_1/a$*.

ARTICLE

For both **1** and **2** at 298 K, both terminal thiophenes on the terthiophene backbones are disordered in a manner common to terminal thiophenes associated with a rotation of about 180°. However, at 100 K, for both **1** and **2** the disorder of the terminal thiophenes was suppressed as the rotation was frozen out. For **1**, none of the terminal thiophenes were disordered in the polymorphic phase at 100 K. For **2** at 100 K, only one of the two terminal thiophenes in both independent molecules in the asymmetric unit were disordered. Further details are provided in the Experimental section.

Table 2. Selected bond lengths for the major component in **1** and **2** at 100 K and 298 K.

M=	Rh (**1**)		Ir (**2**)	
Temperature (K)	100	298	100	298
M-I (Å)	2.6709(5) 2.6618(10)	2.6478(8)	2.648(4) 2.621(2)	2.537(2)
M-$C_{carbene}$ (Å)	2.006(3) 1.961(4)	1.986(5)	2.063(7) 2.002(6)	1.980(4)
N_1-$C_{carbene}$ (Å)	1.357(4) 1.377(4)	1.371(6)	1.310(8) 1.391(8)	1.368(5)
N_2-$C_{carbene}$ (Å)	1.363(4) 1.357(4)	1.354(6)	1.384(8) 1.355(7)	1.366(5)

Table 3. Selected bond angles for the major component in **1** and **2** at 100 K and 298 K.

M=	Rh (**1**)		Ir (**2**)	
Temperature (K)	100	298	100	298
N_2-$C_{carbene}$-N1 (°)	107.3(3) 106.6(3)	106.8(4)	109.2(5) 106.7(5)	107.1(3)
$C_{carbene}$-M-I (°)	83.09(9) 84.77(10)	84.98(15)	83.92(19) 86.49(18)	89.88(14)

Tables 2 and 3 show selected bond angles and lengths, for the components with higher site occupancy in **1** and **2** respectively at each temperature. For **1**, bonds connected to the Rh are virtually unchanged at the two different temperatures, but the C-Rh-I bond angle increased by 1° upon cooling from 298 K to 100 K. Metric parameters for the imidazol-2-ylidene moiety in **1** changed little for both the N-C bond length and N-C-N bond angle. For **2**, the Ir-I and Ir-$C_{carbene}$ distances become elongated upon cooling from 298 K to 100 K, with the C-Ir-I bond angle decreasing from 89.9° to 83.9° and 86.5° for each molecule in the asymmetric unit. The two N-C bond distances in the imidazol-2-ylidene moiety are very similar at 298 K. At 100 K these two bonds became slightly different and the N-C-N bond angle varied from 107.1° at 298 K to 106.7 ° and 109.2° for each molecule in the asymmetric unit. This can be attributed to a slight loss of π-conjugation at 100 K.

Determination of the transition temperature

The approximate transition temperature between the two enantiotropic forms for each compound was also determined. We first studied the powder X-ray diffraction patterns of polycrystalline **1** at 100 K and 298 K and compared them to simulated patterns generated from single crystal data at each temperature (Fig. S1). The differences among these patterns are very minor and we concluded that the transition temperatures for these compounds cannot be tracked easily using powder X-ray diffraction techniques.

An alternative approach using single crystal data proved to be more rewarding. We tracked the transition temperature by monitoring the unit cell symmetry changes (*$P2_1/c(a)$* to *C2c*) on the same crystal. Single crystal data sets for **1** and **2** were collected at varying intervals ranging from 100 K to 298 K (Fig. 2). We used the $N_{(int>3\sigma)}/N_{(total)}$ value to represent how many reflections collected violated a C-centered lattice, as an indication of the symmetry change from *$P2_1/c(a)$* to *C2c* of the crystal. Both $N_{(total)}$ and $N_{(int>3\sigma)}$ values are the values that were subjected to a C-centered lattice exception and were generated by using either CrysAlisPro or XPrep. Fig. 2 shows the percentage value of $N_{(int>3\sigma)}$ / $N_{(total)}$ value plotted versus temperature for **1** and **2** respectively. At higher temperatures (≥150 K), nearly all reflections for **1** and **2** were consistent with a C-centered lattice. Upon cooling to around 140 K, the $N_{(int>3\sigma)}$ / $N_{(total)}$ value of each crystal started to increase slightly. Finally,

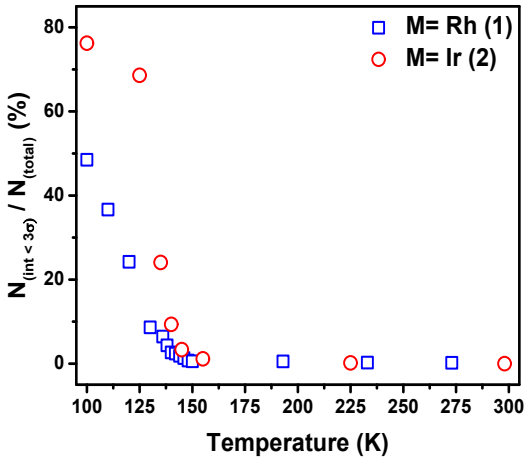

Fig. 2. Percentage of reflections that violated C-centered symmetry (int>3 σ) at different temperature for **1** and **2**.

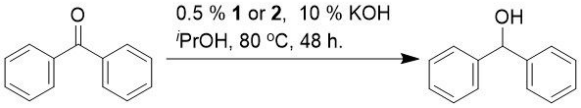

Scheme 2. Hydrogen transfer reactions for **1** and **2**.

when cooled below ≤130 K, the $N_{(int>3\sigma)}$ / $N_{(total)}$ value increased rapidly for both **1** and **2**. For **2**, the number of reflections that violated the C-centered unit cell became saturated at 125 K. By using this method, the phase transition temperatures for the two systems can be narrowed to 138-142 K for **1** and 140-145 K for **2**.

Catalysis of the hydrogen transfer reaction

Ir(cod)I(NHC) was previously reported to catalyze the hydrogen-transfer reaction for the reduction of ketones to the corresponding alcohols.[9] The catalytic activities of **1** and **2** for the hydrogen transfer reaction were tested by reducing benzophenone to diphenylmethanol using ^{i}PrOH as the hydrogen donor (Scheme 2). Both **1** and **2** catalyzed the hydrogen transfer reaction to give the target compound at low catalyst loadings (0.5 %) and in high isolated yield for **2** (94.0 %) and moderate yield for **1** (64.1 %). This demonstrated that the metal complexes featuring the new ligand platform have the potential to be highly active catalyst precursors.

Electropolymerization

Based on previously reported electropolymerizability of the terthiophene moiety[6, 10] and other thiophene derivatives[11] under CV conditions, we then tested the potential polymerization reactions of **1** and **2**. The conducting metallopolymers **poly-1** and **poly-2** were synthesized as orange thin films directly coated onto ITO glass by oxidative electropolymerization of the terthiophene moieties of **1** and **2** respectively (Fig. 3a). Figs. 3b and c show the electropolymerization reaction and representative electropolymerization CV traces of **1** and **2**, respectively**.** The monomer solutions of **1** and **2** in CH_2Cl_2 were tested for 15 CV scans by sweeping the potential using ITO-coated glass as the working electrode, with 0.1 M tetra(*n*-butyl)ammonium hexafluorophosphate ($TBAPF_6$) as supporting electrolyte. The CV plot of **1** (Fig. 3b) revealed one weak Rh-based reversible electron transfer at $E_{1/2}$ = 0.77 V (*vs.* Fc/Fc^+) and two terthiophene-based irreversible electron transfers at $E_{ox.}$ = 1.23 V (*vs.* Fc/Fc^+) and $E_{red.}$ = 0.28 V (*vs.* Fc/Fc^+) for the first scan. The polythiophene-based response emerged at $E_{ox.}$ = 0.71 V (*vs.* Fc/Fc^+) starting with the second scan. Synthesis of **poly-1** was accompanied by sequential growth in current and linear increases of peak current indicating that the amount of deposited polymer on the ITO surface increased with successive CV scans (Fig. 3b inset). Similarly, the CV plot of **2** (Fig. 3c) revealed one Ir-based reversible electron transfer at $E_{1/2}$ = 0.50 V (*vs.* Fc/Fc^+) and one terthiophene-based irreversible electron transfer at $E_{ox.}$ = 1.15 V (*vs.* Fc/Fc^+). The sequential growth in current with a linear increase of peak current again showed that the growth of **poly-2** thin film increased with successive CV

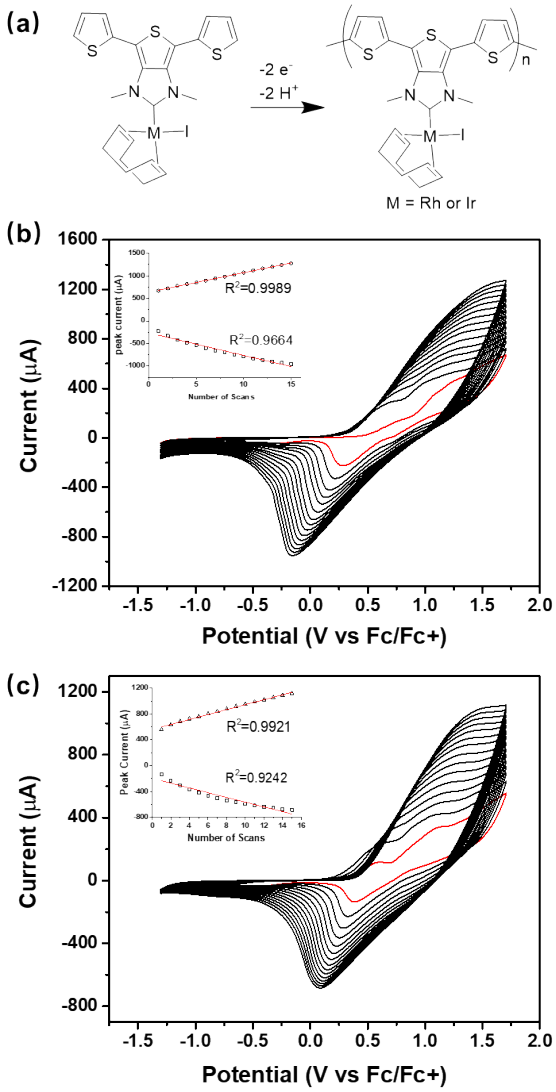

Fig. 3. (a) Synthesis of **poly-1** and **poly-2**. (b) Electropolymerization of **1** in CH_2Cl_2 using a 0.7 mM monomer solution. (c) Electropolymerization of **2** in CH_2Cl_2 using a 0.6 mM monomer solution (b). Insets in (b) and (c) show the linear relationship between current at peak oxidation/reduction potentials and number of scans. All potentials are reported with referenced to Fc/Fc^+ couple as 0 V.

scans (Fig. 3c inset). Freshly synthesized **poly-1** and **poly-2** were then characterized by CV plots in a monomer-free electrolyte solution at different scan rates (Fig. S2). The two polymer films show good stability in CH_2Cl_2. The linear relationship of observed oxidation/reduction peak current with scan rate in the range of 50 mV/s to 250 mV/s demonstrated that both **poly-1** and **poly-2** were highly electroactive porous polymer thin films in which current was not limited by the diffusion of electrolyte ions (Fig. S2 inset).

Compositional analyses on freshly prepared **poly-1** and **poly-2** on ITO-coated glass electrodes were obtained by quantitative X-ray photoelectron spectroscopy (XPS) studies.

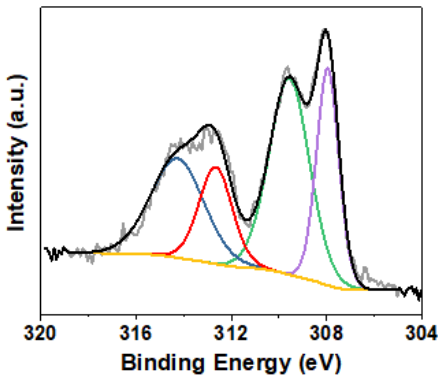

Fig. 4. Deconvoluted Rh 3d XPS spectrum of **poly-1**.

The atomic ratios in **poly-1** were Rh: S: N = 1.0: 3.2: 2.1 which is consistent with the predicted stoichiometric ratios of 1: 3: 2 for the proposed structure. The binding energy and the deconvoluted Rh 3d XPS spectrum revealed that the Rh in **poly-1** was a mixture of Rh(I) and Rh(III) in a 0.63 to 0.37 ratio (Fig. 4). The atomic ratios observed in **poly-1** for Rh: I: P were 1.0: 0.38: 1.66, where the P signal was due to the PF_6^- anion in the CMP. Cumulatively, Rh gave a total cation charge of 2.26 (Rh(I) and Rh(III)) compared to a total anion charge of 2.04 from both I^- and PF_6^- species, per repeating unit. This indicates **poly-1** can be considered as charge-balanced polymer thin film. For **poly-2**, the atomic ratios were Ir: S: N = 1.0: 2.6: 2.1. which matches the predicted stoichiometric ratio of 1:3:2 in the proposed structure. All the other deconvoluted XPS spectra of specific elements with the binding energy for **poly-1** and **poly-2** can be found in Figs. S3 and S4 respectively. The XPS results confirmed the formation of the desired metallopolymers coated onto ITO-glass surfaces.

Electrochromic studies

Poly-1 and **poly-2** displayed color changes under applied potentials due to the generation of charge transport species (polaron and bipolaron). This phenomenon has been observed in other terthiophene-based metallopolymer systems.[1, 2b, 2c, 6a] The electrochromic properties of **poly-1** and **poly-2** on ITO-coated glass were studied by UV-vis-NIR spectroelectrochemistry in CH_2Cl_2 electrolyte solutions. Electrochromic properties of **poly-1** and **poly-2** resemble those of the previously reported Pd and Pt complexes using the same organic polymer scafford.[7] Fig. 5 summarizes the absorption spectra of **poly-1** and **poly-2** at different applied voltages and the corresponding color changes observed by the naked eye. Freshly prepared **poly-1** was light yellow with an absorption maximum at 423 nm which can be assigned to the π-π* transition. When partially oxidized, the film turned to light green. Two additional absorption bands emerged at 745 nm and 1310 nm which were assigned to polaron transitions with the intensity of the neutral state π-π* transferred to those polaron transitions. In the fully oxidized state, the neutral state π-π* transition is depleted. Two polaron bands further combine into one bipolaron band centered at 1032 nm which tails into the

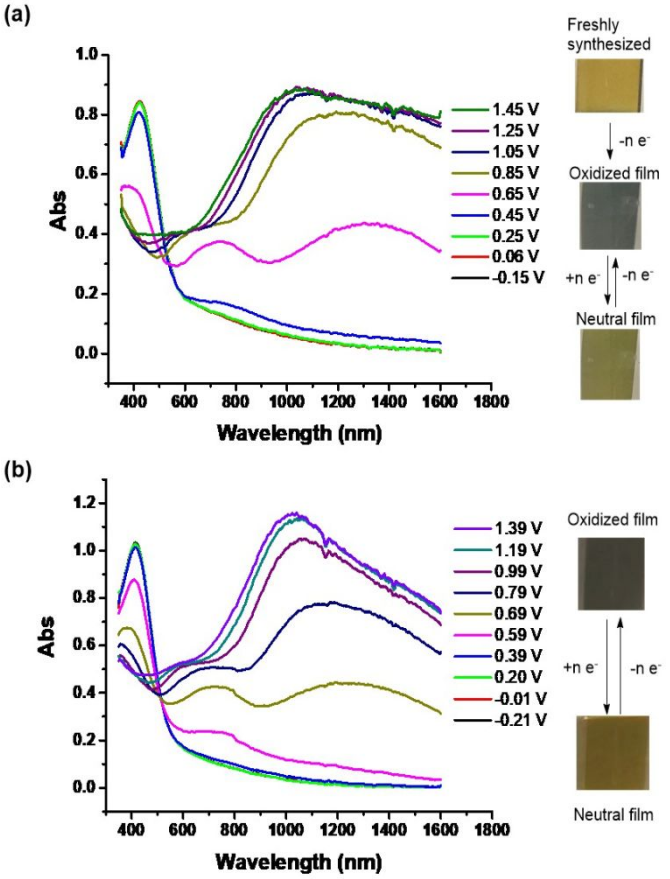

Fig. 5. UV-vis-NIR spectroelectrochemical spectra on ITO-coated glass substrates at different applied potentials in CH_2Cl_2 electrolyte solution for **poly-1** (a) and **poly-2** (b)**.** All potentials are reported with referenced to Fc/Fc^+ couple as 0 V.

red region. The resulting oxidized **poly-1** was light blue. One explanation is that by further increasing the applied potential on partially oxidized **poly-1** additional electrons are removed from existing polarons (radical cations) and this generates new bipolarons (cations) instead of generating new polarons from other regions of the neutral polymer backbone. Upon reduction to 0 V (*vs.* Ag/Ag^+), **poly-1** only restored back to the partially oxidized state. The color change of **poly-1** can be reversed up to 100 cycles when being continuously cycled with an applied potential from 0 V to 1.5 V (*vs.* Ag/Ag^+).

Similar to **poly-1**, neutral **poly-2** was also light yellow with a π-π* transition at 415 nm. The polaron absorption bands emerged at 755 nm and 1270 nm in the partially oxidized state. The fully oxidized **poly-2** thin film was dark blue in color. Only one broad bipolaron absorption centered at 1023 nm can be observed, with the complete depletion of the neutral state π-π* transition. Under continuously cycling applied potential from 0 V to 1.5 V (*vs.* Ag/Ag^+), the color reversibility of **poly-2** maintained for 11 cycles and the wet film stayed fully oxidized even when taken out of the electrolyte solution. For the Ir-based **poly-2**, its electromic behavior is similar to that of the previously reported metallopolymers which incorporate an

NHC-Ir metal complex, with a similar color change based on polaron/bipolaron generation.[1]

Conclusions

In summary, new Rh(TThMe)(cod)I and Ir(TThMe)(cod)I complexes with a terthiophene backbone were synthesized, and their structures were confirmed by single crystal X-ray diffraction studies. Their enantiotropic forms at 100 K and 298 K were characterized by single crystal X-ray diffraction studies showing that both forms have similar cell parameters with different space groups (*P21/c(a)* at 100 K and *C2/c* at 298 K). Rapid single crystal X-ray diffraction scans were used to track the symmetry changes in order to establish the transition temperatures which were around 140 K for both **1** and **2**. The electropolymerization of both complexes was achieved on ITO-coated glass and the conducting metallopolymers **poly-1** and **poly-2** were prepared and characterized by CV and quantitative XPS studies. UV-vis-NIR spectroelectrochemistry studies of **poly-1** and **poly-2** revealed that charge transport species (polarons and bipolorans) were generated along the polythiophene backbone upon oxidation leading to a color change of each thin film. Future studies of conducting metallopolymers will focus on the synthesis of more electropolymerizable transition metal complexes and their novel structural features as well as intrinsic catalytic and electronic properties.

Experimental

General method

Air- and moisture-sensitive reactions were carried out using standard Schlenk techniques. Tetrahydrofuran (THF) and CH_2Cl_2 used in air-sensitive handling/reactions and all electrochemical experiments were dried via a two-column alumina purification system (Pure Process Technology, NH) and then degassed by purging under N_2 for 1 h before stored over activated 3Å molecular sieves. Isopropyl alcohol (^{i}PrOH) was distilled over anhydrous $CaCl_2$ and stored over activated 3Å molecular sieves. Tetrabutylammonium hexafluorophosphate ($TBAPF_6$) was purchased from Oakwood and purified by triplicate recrystallization from hot ethanol before drying under a dynamic vacuum for three days. ITO-coated glasses (Rs = 70−100 Ω, 7 × 50 × 0.7 mm) were purchased from Delta Technologies, LTD and were cleaned by sonicating sequentially in acetone and dichloromethane prior to use. All the other chemicals were purchased from commercial sources and used without further purification.

Characterization

^{1}H NMR spectra were recorded using a Bruker AVANCE III 500 MHz NMR at 500 MHz. Coupling constants are reported in hertz (Hz), and chemical shifts are reported as parts per million (ppm) relative to residual solvent peaks (residual CD_2Cl_2 δH = 5.32) or tetramethylsilane (δH = 0).[12] ^{13}C NMR spectra were recorded using a Bruker AVANCE III 500 MHz NMR at 125 MHz. Chemical shifts are reported as parts per million (ppm) relative to residual solvent peaks (residual CD_2Cl_2 δC = 53.84) or tetramethylsilane (δC = 0).[12] High resolution mass spectra (HR-MS) were obtained on an Agilent Technologies 6530 Accurate Mass Q-TOF LC/MS instrument. Infrared spectra were recorded with a Nicolet IR 200 FTIR spectrophotometer. XPS spectra were collected using a Kratos X-ray Photoelectron Spectrometer with a monochromatic Al K*α* source (1486.7 eV). Melting points were recorded with an OptiMelt Automated Melting Point System with digital image processing technology from Stanford Research System (SRS, Sunnyvale, CA) and uncorrected values are reported.

Electrochemistry

Electrochemical studies were performed in a glove-box under an N_2 atmosphere using GPES software from Eco. Chemie B. V. and an Autolab Potentiostat (PGSTAT30). All electrochemical experiments were performed with 0.1 M tetrabutylammonium hexafluorophosphate ($TBAPF_6$) as supporting electrolyte. All cyclic voltammetry experiments were carried out with an ITO-coated glass as the working electrode, a Pt wire coil counter electrode and an $Ag/AgNO_3$ reference electrode (silver wire dipped in a 0.01 M silver nitrate solution with 0.1 M $TBAPF_6$ in dry acetonitrile). The ferrocene/ferrocenium couple (Fc/Fc^+) was used as an external standard to calibrate the reference electrode.

Single Crystal X-ray diffraction

Suitable crystals were selected, covered with hydrocarbon oil and mounted on the tip of a nylon fiber. Data set at 298 K of **1** and **2** were collected on a Nonius Kappa CCD diffractometer with a Bruker AXS Apex II detector and an Oxford Cryosystems 700 low-temperature device, using a graphite monochromator with MoKα (λ = 0.71075 Å). Data sets at 100 K of **1** and **2** and the temperature dependent measurements were collected on an Agilent Technologies SuperNova Dual Source diffractometer with an AtlasS2 CCD detector and an Oxford 700 low-temperature attachment, using a μ-focus Cu Kα radiation source (λ = 1.5418 Å) with collimating mirror monochromators. Details of crystal data, data collection and structure refinement are listed in Table 1. Using Olex2[13], the structures were solved with the ShelXT[14] structure solution program using Intrinsic Phasing and refined with the ShelXL[15] refinement package using Least Squares minimization.

The disorder for all thiophene groups was modeled in essentially the same way. For example, for one of the thiophene rings, the site occupancy factor for the atoms of one component of the disorder was set to the variable x. The site occupancy factors for the atoms of the alternate component was set to (1-x). The geometry of the two components was restrained to be equivalent throughout the refinement process. A common isotropic displacement parameter was refined while refining x. With the convergence of the value for x, the site occupancies were fixed, and the displacement parameters were allowed to refine while restraining their values to be both similar and approximately isotropic (SIMU and ISOR instructions).

For determination of the crystal symmetry, the quick single crystal data set collection in the temperature range of 100-273 K are conducted in the aforementioned Agilent Technologies SuperNova Dual Source diffractometer with an AtlasS2 CCD detector and an Oxford 700 low-temperature attachment, using a μ-focus Cu Kα radiation source (λ = 1.5418 Å) with collimating mirror monochromators. For **1**, approximatly 28000 reflections were collected at the higher temperature ranges (193 to 273 K) in approximatly 2.5 hours data collection time, and approximatly 16100 reflections were collected in the lower temperature range (100 K to 153 K) in approximatly 2 hours data collection time. For **2**, approximatly 15600 reflections were collected for all temperatures in approximatly 2 hours data collection time.

Powder X-ray diffraction (PXRD)

PXRD experiments were collected on an Agilent Technologies SuperNova Dual Source diffractometer with an AtlasS2 CCD detector and an Oxford 700 low-temperature attachment, using a μ-focus Cu Kα radiation source (λ = 1.5418 Å) with collimating mirror monochromators. Data were collected in the range of 4–50° 2θ. Simulated PXRD patterns were generated using single crystal reflection data via the SimPowPatt utility in PLATON[16].

Spectroelectrochemistry

The *in-situ* UV-vis−NIR absorption-based spectro-electrochemical measurements were performed using the cell arrangement described above with a polymer film electrochemically deposited on indium−tin−oxide (ITO)-coated glass substrate as the working electrode, a platinum wire as the counter electrode, and an $Ag/AgNO_3$ reference electrode. Experiments were carried out in an optical cuvette inside an inert atmosphere (N_2) glovebox. Absorption spectra were recorded on a Varian Cary 6000i UV-vis-NIR spectrophotometer within the NIR/vis spectral region (1600 ≥ λ ≥ 350 nm) under several applied potentials.

Compound Synthesis.

1, (Rh(TThMe)(cod)I): To an oven-dried 10-mL Schlenk flask with a magnetic stir bar was added **L**[7] (60.0 mg, 0.14 mmol, 1 equiv.), KO^{t}Bu (16.8 mg, 0.15 mmol, 1.1 equiv.) and $[Rh(cod)Cl]_2$[17] (35.8 mg, 0.073 mmol, 0.54 equiv.). The solid was dried under vacuum for 1 hour before suspended with dry THF (5 mL). The mixture was stirred at 60 °C for 16 hours. After cooling to room temperature, the mixture was filtered with celite under air and further eluted with THF. The solvent volume was then reduced to about 1 mL by rotary evaporation. The resulting mixture was then precipitated by layering Et_2O (12 mL) and cooling (-20 °C). The precipitate was then collected via centrifuge and further washed with Et_2O (2 x 5 mL) to give the target compound as a pale orange solid. Yield, 51.0 mg, 58%: ^{1}H NMR (500 MHz, $CDCl_3$) δ 7.41 (dd, *J* = 5.2, 1.2 Hz, 2H), 7.16 (dd, *J* = 3.6, 1.2 Hz, 2H), 7.09 (dd, *J* = 5.2, 3.5 Hz, 2H), 5.33 (t, *J* = 3.6 Hz, 2H), 4.04 (s, 6H), 3.59 – 3.54 (m, 2H), 2.34 (dd, *J* = 9.9, 3.4 Hz, 4H), 2.07 – 1.96 (m, 2H), 1.90 – 1.83 (m, 3H). ^{13}C NMR (125 MHz, $CDCl_3$) δ 212.63, 136.55, 130.81, 129.23, 1207.65, 127.59, 106.38, 99.00, 98.95, 72.24, 72.13, 36.99, 32.26, 29.72, 29.43. HR-MS (ESI+): $[M-I]^+$ ($C_{23}H_{24}N_2RhS_3^+$), calcd.: 527.0151, found: 527.0143. FT-IR (cm^{-1}): 3386 (br, w), 3067 (w), 3019 (w), 2918 (w), 2972 (w), 2850 (w), 2828 (w), 1718 (w), 1676 (w), 1569 (m), 1449 (m), 1419 (m), 1408 (m), 1351 (m), 1302 (w), 1285 (m), 1229 (w), 1178 (w), 1124 (w), 1069 (s), 1040 (m), 994 (m), 951 (m), 928 (m), 866 (w), 848 (m), 831 (m), 807 (m), 784 (w), 697 (s), 591 (w), 573 (m), 524 (m), 500 (s), 479 (s), 436 (m). m.p.: 215 °C (decomp.). Crystals suitable for single crystal X-ray diffraction studies were grown from a concentrated solution of **1** in THF by layering with Et_2O and cooling to -20 °C.

2, (Ir(TThMe)(cod)I): To an oven-dried 25-mL Schlenk flask with a magnetic stir bar was added **L** (99.7 mg, 0.22 mmol, 1 equiv.), KO^{t}Bu (28.0 mg, 0.25 mmol, 1.1 equiv.) and $[Ir(cod)Cl]_2$[18] (81.7 mg, 0.12 mmol, 0.54 equiv.). The solid was dried under vacuum for 1 hour before suspended with dry THF (10 mL). The mixture was then stirred at 65 °C for 16 hours. After cooling to room temperature, the mixture was filtered with celite under air and further eluted by THF. The solvent was then removed by rotary evaporation. The target compound was collected by recrystallizing the resulting black solid from a mixture of CH_2Cl_2 (3 mL) and pentane (15 mL) as a dark solid. Yield, 108 mg, 65%: ^{1}H NMR (500 MHz, CD_2Cl_2) δ 7.45 (d, *J* = 5.1 Hz, 2H), 7.20 (d, *J* = 3.5 Hz, 2H), 7.12 (dd, *J* = 5.2, 3.6 Hz, 2H), 4.87 – 4.80 (m, 2H), 3.91 (s, 7H), 3.14 – 3.08 (m, 2H), 2.26 – 2.10 (m, 4H), 1.92 – 1.76 (m, 2H), 1.50 – 1.41 (m, 2H). ^{13}C NMR (125 MHz, CD_2Cl_2): δ 207.00, 137.15, 131.27, 129.67, 128.09, 128.02, 107.09, 86.05, 56.16, 36.75, 33.14, 30.48. FT-IR (cm^{-1}): 3453 (br, w), 3076 (w), 3012 (w), 2915 (m), 2875 (m), 2830 (m), 2006 (br, w), 1721 (w), 1680 (m), 1556 (m), 1447 (m), 1435 (m), 1421 (m), 1405 (m), 1351 (s), 1338 (s), 1286 (m), 1228 (m), 1175 (m), 1122 (w), 1066 (s), 1040 (m), 1002 (m), 953 (m), 930 (m), 847 (m), 831 (s), 697 (s), 575 (w), 528 (m), 499 (m), 468 (m). m.p. 256 °C (decomp.). Crystals suitable for single crystal X-ray diffraction study were grown from a concentrated solution of **2** in CH_2Cl_2 by layering with pentane and cooling to -20 °C.

The catalytic reaction for the hydrogen-transfer reaction

To a 25 mL oven-dried Schlenk tube with a magnetic stir bar, benzophenone (365 mg, 2 mmol, 1 equiv.), ground KOH (11.2 mg, 0.20 mmol, 0.1 equiv.) and the catalyst (**1**: 6.8 mg, **2**: 7.8 mg, 0.01 mmol, 0.5 %) were added and the mixture dried under vacuum for 1 h. The solids were then dissolved in dry ^{i}PrOH (5 mL) and the flask was capped with a glass stopper, followed by stirring at 80 °C for 50 h before cooling to room temperature. The resulting mixture was filtered through a short column of Celite and further eluted with additional CH_2Cl_2 (10 mL). The solvent was then removed by rotary evaporation. The resulting solid was purified on a silica gel column using a mixture of hexanes and CH_2Cl_2 (1:4) as eluent to give the product as a white powder. Yield, **1**: 236 mg, 64.1 %; **2**: 347 mg, 94.0%: ^{1}H NMR (500 MHz, $CDCl_3$) δ 7.37 – 7.28 (m, 8H), 7.27 – 7.20 (m, 2H), 5.78 (d, *J* = 3.4 Hz, 1H), 2.36 (d, *J* = 3.5 Hz, 1H). ^{13}C NMR (125 MHz, $CDCl_3$): δ 143.91, 128.59, 127.66, 76.32. The spectroscopic data matches the previously reported literature values.[19]

Conflicts of interest

There are no conflicts to declare.

Acknowledgements

The purchase of the Bruker AVANCE III 500 spectrometer was made possible with NIH funding (1 S10 OD021508-01). We thank the Welch Foundation for support (F-816). We acknowledge the NSF (CHE-1807847) for support.

Notes and references

1. Arduengo, A. J.; Harlow, R. L.; Kline, M., *J. Am. Chem. Soc.* **1991,** *113*, 361-363.
2. (a) Powell, A. B.; Bielawski, C. W.; Cowley, A. H., *J. Am. Chem. Soc.* **2009,** *131*, 18232-18233; (b) Powell, A. B.; Bielawski, C. W.; Cowley, A. H., *J. Am. Chem. Soc.* **2010,** *132*, 10184-10194; (c) Satheeshkumar, C.; Park, J.-Y.; Jeong, D.-C.; Song, S. G.; Lee, J.; Song, C., *RSC Adv.* **2015,** *5*, 60892-60897.
3. (a) Haleblian, J.; McCrone, W., *J. Pharm. Sci.* **1969,** *58*, 911-929; (b) Rosenstein, S.; Lamy, P. P., *Am. J. Health-Syst. Pharm.* **1969,** *26*, 598-601.
4. Raza, K., *SOJ Pharm. Pharm. Sci.* **2014**.
5. Braga, D.; Grepioni, F., *Chem. Soc. Rev.* **2000,** *29*, 229-238.
6. (a) Nguyen, M. T.; Jones, R. A.; Holliday, B. J., *Chem. Commun.* **2016,** *52*, 13112-13115; (b) Reddinger, J. L.; Reynolds, J. R., *Macromolecules* **1997,** *30*, 673-675; (c) Reddinger, J. L.; Reynolds, J. R., *Chem. Mater.* **1998,** *10*, 3-5; (d) Reddinger, J. L.; Reynolds, J. R., *Chem. Mater.* **1998,** *10*, 1236-1243.
7. Wang, W.; Guo, H.; Jones, R. A., *Dalton Trans.* **2019,** *48*, 14440-14449.
8. Farrugia, L. J., *J. Appl. Crystallogr.* **2012,** *45*, 849-854.
9. Zinner, S. C.; Rentzsch, C. F.; Herdtweck, E.; Herrmann, W. A.; Kuhn, F. E., *Dalton Trans.* **2009**, 7055-7062.
10. (a) Djukic, B.; Lemaire, M. T., *Inorg. Chem.* **2009,** *48*, 10489-10491; (b) Sun, C.; Prosperini, S.; Quagliotto, P.; Viscardi, G.; Yoon, S. S.; Gobetto, R.; Nervi, C., *Dalton Trans.* **2016,** *45*, 14678-14688; (c) O'Sullivan, T. J.; Djukic, B.; Dube, P. A.; Lemaire, M. T., *Chem. Commun.* **2009**, 1903-1905.
11. (a) Yu, H. H.; Xu, B.; Swager, T. M., *J. Am. Chem. Soc.* **2003,** *125*, 1142-1143; (b) Tovar, J. D.; Swager, T. M., *Adv. Mater.* **2001,** *13*, 1775-1780; (c) Kingsborough, R. P.; Swager, T. M., *J. Am. Chem. Soc.* **1999,** *121*, 8825-8834; (d) Song, C.; Swager, T. M., *Macromolecules* **2005,** *38*, 4569-4576; (e) Holliday, B. J.; Stanford, T. B.; Swager, T. M., *Chem. Mater.* **2006,** *18*, 5649-5651; (f) Djukic, B.; Seda, T.; Gorelsky, S. I.; Lough, A. J.; Lemaire, M. T., *Inorg. Chem.* **2011,** *50*, 7334-7343.
12. Fulmer, G. R.; Miller, A. J. M.; Sherden, N. H.; Gottlieb, H. E.; Nudelman, A.; Stoltz, B. M.; Bercaw, J. E.; Goldberg, K. I., *Organometallics* **2010,** *29*, 2176-2179.
13. Dolomanov, O. V.; Bourhis, L. J.; Gildea, R. J.; Howard, J. A. K.; Puschmann, H., *J. Appl. Cryst.* **2009,** *42*, 339-341.
14. Sheldrick, G. M., *Acta Cryst. A* **2015,** *71*, 3-8.
15. Sheldrick, G. M., *Acta Cryst. C* **2015,** *71*, 3-8.
16. Spek, A. L., *Acta Crystallogr. D Biol. Crystallogr.* **2009,** *65*, 148-155.
17. Giordano, G. C., R. H., *Inorg. Synth.* **1979,** *19*, 218-220.
18. Herde, J. L. L., J. C.; Senoff, C. V., *Inorg. Synth.* **1974,** *15*, 18-20.
19. Tamang, S. R.; Findlater, M., *J. Org. Chem.* **2017,** *82*, 12857-12862.